

# Spontaneous separation of bi-stable biochemical systems into spatial domains of opposite phases

J. Elf<sup>†</sup> and M. Ehrenberg

**Abstract:** Bi-stable chemical systems are the basic building blocks for intracellular memory and cell fate decision circuits. These circuits are built from molecules, which are present at low copy numbers and are slowly diffusing in complex intracellular geometries. The stochastic reaction-diffusion kinetics of a double-negative feedback system and a MAPK phosphorylation-dephosphorylation system is analysed with Monte-Carlo simulations of the reaction-diffusion master equation. The results show the geometry of intracellular reaction compartments to be important both for the duration and the locality of biochemical memory. Rules for when the systems lose global hysteresis by spontaneous separation into spatial domains in opposite phases are formulated in terms of geometrical constraints, diffusion rates and attractor escape times. The analysis is facilitated by a new efficient algorithm for exact sampling of the Markov process corresponding to the reaction-diffusion master equation.

## 1 Introduction

Biochemical systems can be in different, self-perpetuating states depending on previous stimuli [1–3]. Such biochemical memory is exemplified by the irreversible developmental switches in the cell cycle [4], the maturation of oocytes [5], the on-off switches in gene-activity [6], and the ubiquitous phosphorylation switches in signal transduction pathways [7]. The dynamical properties of such systems often defy intuition, and their analysis requires mathematical modelling [8]. To account for random transitions between states, stochastic descriptions of the chemical reactions are necessary [9, 10] and to account for the cell geometry and slow intracellular diffusion, spatial considerations are mandatory [11, 12]. In a recent experimental study [13] it was demonstrated that bistability can vanish due to spatially localised fluctuations for inorganic catalysts, and thus invalidate any macroscopic description of the kinetics. The present study addresses consequences of similar kinetic behaviour in intracellular biochemical systems.

Two bi-stable model systems serve to exemplify the stochastic and spatial aspects of intracellular signalling. The results reveal that the average times for random transitions between two self-perpetuating states are reduced by finite diffusion rates, and suggest a general rule for the spontaneous emergence of spatial domains in opposite states and loss of global bistability. The findings disclose previously unknown physical constraints on the design of intracellular control circuits that depend on stable attractors, and fill a gap in the current knowledge of spatially heterogeneous bi-stable systems.

Stochastic models for intracellular kinetics are gaining in importance for the interpretation of *in vivo* experiments [14, 15]. These models are commonly based on the

homogeneous chemical master equation (ME) for well stirred systems [10, 16]. This approximation, where the state of the system is defined by the total copy numbers of the different reactants, is only valid if equilibration between the microstates of the reactants, thermal equilibration between the reactants and the solvent, and equilibration of the reactants between all positions in the system volume occur on a much faster timescale than the chemical reactions [10].

Since diffusion of molecules in a living cell is considerably slower than in the test tube [17], the condition of spatial homogeneity is expected to be violated in many cases. In fact, many important intracellular processes depend on spatial heterogeneity [11, 12]. Among these are cell division [18], morphogenesis [19], local signal processing in neurons [20], and some types of chemotaxis [21].

A feasible starting point for stochastic descriptions of spatially heterogeneous systems is to divide the reaction volume into a finite number of subvolumes and apply the reaction diffusion master equation (RDME or multivariate master equation) [9, 22, 23]. The state of such a system is defined by the copy numbers of all reactants in each artificial subvolume, which must be chosen small enough to ensure homogeneity [23]. Diffusion is accounted for as first-order elementary reactions for the exchange of molecules between subvolumes. The rate constants are  $D/l^2$ , where  $D$  is the diffusion constant for a particular reactant and  $l$  is the side length of the cubic subvolume [9, 23].

Stochastic analyses of spatially extended bi-stable systems are difficult for two reasons. Firstly, the complexity of the RDMEs makes analytical solutions hard to come by and secondly, direct numerical solutions are impossible due to the large state space. Accordingly, there exists but a handful of RDME descriptions of bi-stable non-equilibrium systems in 1D [23, 24], and none in 2D or 3D, where the most interesting biological problems reside. Furthermore, the properties of bi-stable systems in 2D and 3D cannot be inferred from 1D considerations. The reason is that curvature of domain fronts, which is important for macroscopic system dynamics in 2D and 3D [25, 26], is missing in 1D.

The present RDME-analysis of stochastic reaction diffusion kinetics in 3D was made possible by the

development of a new algorithm, the Next Subvolume Method (NSM), which is described in the next Section.

## 2 Results

### 2.1 The Next Subvolume Method

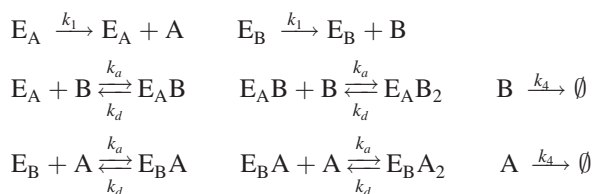
When the chemical reactions in an intracellular 3D system are fast in relation to diffusion, the subvolumes used in the RDME must be small and their number correspondingly large (several millions) to ensure spatial homogeneity of the reactants in the subvolumes on the time scale of the chemical reactions. In such cases, direct application of Gillespie's algorithm [27] for Monte Carlo simulations of the ME is not feasible, due to the linear relation that exists between the number of subvolumes and the computational effort. This has prevented such approaches to 2D and 3D systems, while 1D simulations of the RDME were pioneered already in 1979 [28]. Progress in stochastic simulations of 3D biological systems was reached in the SmartCell project [29–31] by the application of the Next Reaction Method [32] to spatial problems.

We have designed an efficient MC algorithm, the Next Subvolume Method (NSM), that samples trajectories of the Markov process corresponding to the RDME (see Supplementary Methods). The trajectories are therefore equivalent to those obtained with Gillespie's Direct Method [27]. The algorithm has been tailor-made for the RDME and the computation times scale logarithmically, rather than linearly, with the number of subvolumes. Accordingly, statistically significant results for systems that require millions of subvolumes can now be obtained with standard PCs. This leap in computational efficiency originates in a combination of the Direct Method [27] for sampling the time for a next reaction or diffusion event in each subvolume, with Gibson and Bruck's Next Reaction Method [32], which is used to keep track of in which subvolume an event occurs next. The subvolumes are kept sorted in a queue, implemented as a binary tree, according to increasing time of the next event. When an event has occurred in the subvolume at the top of the queue, new event times need to be sampled only for one (the event is a chemical reaction) or two (the event is a diffusion jump) subvolume(s).

When the number of subvolumes is large, the NSM is more efficient than a direct application of the Next Reaction Method (NRM) to the RDME (see Supplementary Methods).

### 2.2 Spontaneous domain separation in bi-stable systems with slow diffusion

We first analyse a bi-stable biochemical system built on the double-negative feedback principle [2]. Two enzymes,  $E_A$  and  $E_B$ , synthesise two different compounds, A and B, respectively. The A molecules inhibit the activity of  $E_B$  and the B molecules inhibit the activity of  $E_A$ . Free A and B molecules are eliminated with the same first-order rate constant. When  $E_A$  and  $E_B$  have the same kinetic parameters, the system is symmetric with respect to A and B.



The double-negative feedback scheme. In the limit of fast diffusion, the parameters used in this study are:  $[E_A]_{\text{tot}} = [E_B]_{\text{tot}} = 12.3 \text{ nM}$  (200 molecules in 27 femtoliters),  $k_1 = 150 \text{ s}^{-1}$ ,  $k_a = 1.2 \cdot 10^8 \text{ s}^{-1} \text{ M}^{-1}$ ,  $k_d = 10 \text{ s}^{-1}$ ,  $k_4 = 6 \text{ s}^{-1}$ .

The RDME and the macroscopic reaction diffusion equations for the scheme are given in the online supplementary text A. The total system volume and diffusion rates are varied as described in the text. The diffusion constant,  $D$ , is set equal for all components and all reactions given in the scheme are approximated as single-step transitions. Association and dissociation rate constants are partially diffusion controlled [33], meaning that they increase towards asymptotes with increasing diffusion constants. At finite diffusion rates, the association and disassociation rate constants were modified accordingly (see online supplementary text B). The inevitable coupling between free diffusion and chemical kinetics makes it difficult to simplify detailed reaction schemes without distorting the overall properties of the system or making physically unsound assumptions.

In Fig. 1a, the correlation time ( $\tau_c$ ) for the number  $n_A$  of A molecules is plotted as a function of the linear extension of the system for different diffusion constants.  $\tau_c$  is the time  $\tau$  at which the normalised autocorrelation function  $\langle n_A(t)n_A(t+\tau) \rangle / \langle n_A \rangle^2 - 1$  has decreased to  $e^{-1}$  of its value at  $\tau = 0$ . (The correlation time is one-half of the average time of escape from one of the attractors in a symmetric bistable system). When diffusion is infinitely fast, so that the system is homogenous and can be described by the ordinary ME, the correlation time increases approximately exponentially with the volume of the system (Fig. 1a, black line). When, in this fast diffusion case, the volume goes to infinity, the rate of escape from an attractor becomes zero. In this macroscopic limit, the system is truly bi-stable.

When the diffusion constants are finite, the  $\tau_c$  values deviate significantly from those in the homogenous case: when the system volume is small, the correlation times are longer and when the system volume is large, they are shorter than in the homogenous case. The reason why they are longer for small volumes can be traced to the slower reaction kinetics of homogenous systems with finite, as opposed to infinite diffusion rate [33]. The reason why, in large volumes, systems with finite diffusion rates have shorter correlation times than systems with infinite diffusion rates is more interesting: it has to do with domain separations that emerge when the reactants have finite diffusion rates.

For the intermediary diffusion constants (Fig. 1a, green and blue lines), the correlation time increases approximately exponentially with the volume, albeit with smaller slopes than in the limit of infinite diffusion rate (Fig. 1a, black line). For the smallest diffusion constant, however, the correlation time reaches a plateau where it remains constant, in spite of further volume increase (Fig. 1a, red line). Simulations of the total numbers of A and B molecules in the system are also shown in Fig. 1a (inserts). At a system volume of  $2.5^3 \mu\text{m}^3$ , the distance between the attractors, as measured by the absolute value of the difference between the average numbers of A and B molecules, is largest in the case of infinite diffusion constants and decreases monotonically with decreasing diffusion rates. The reduced difference between the attractors results in ever faster jumps between them.

Further understanding of these events comes from snap-shots showing how the numbers of A (red dots) and B (blue dots) molecules are distributed in a large volume ( $V = 6^3 \mu\text{m}^3$ ) for systems with slow ( $D = 2 \cdot 10^{-9} \text{ cm}^2 \text{ s}^{-1}$ ) and intermediate ( $D = 5 \cdot 10^{-9} \text{ cm}^2 \text{ s}^{-1}$ ) diffusion rates (Fig. 1b). Initially, there are only A molecules in the system and in the slow diffusion case, where there is a distinct plateau in Fig. 1a, the system rapidly separates into domains of opposite phases. This means that the system is in different attractors in different parts of the volume, which explains

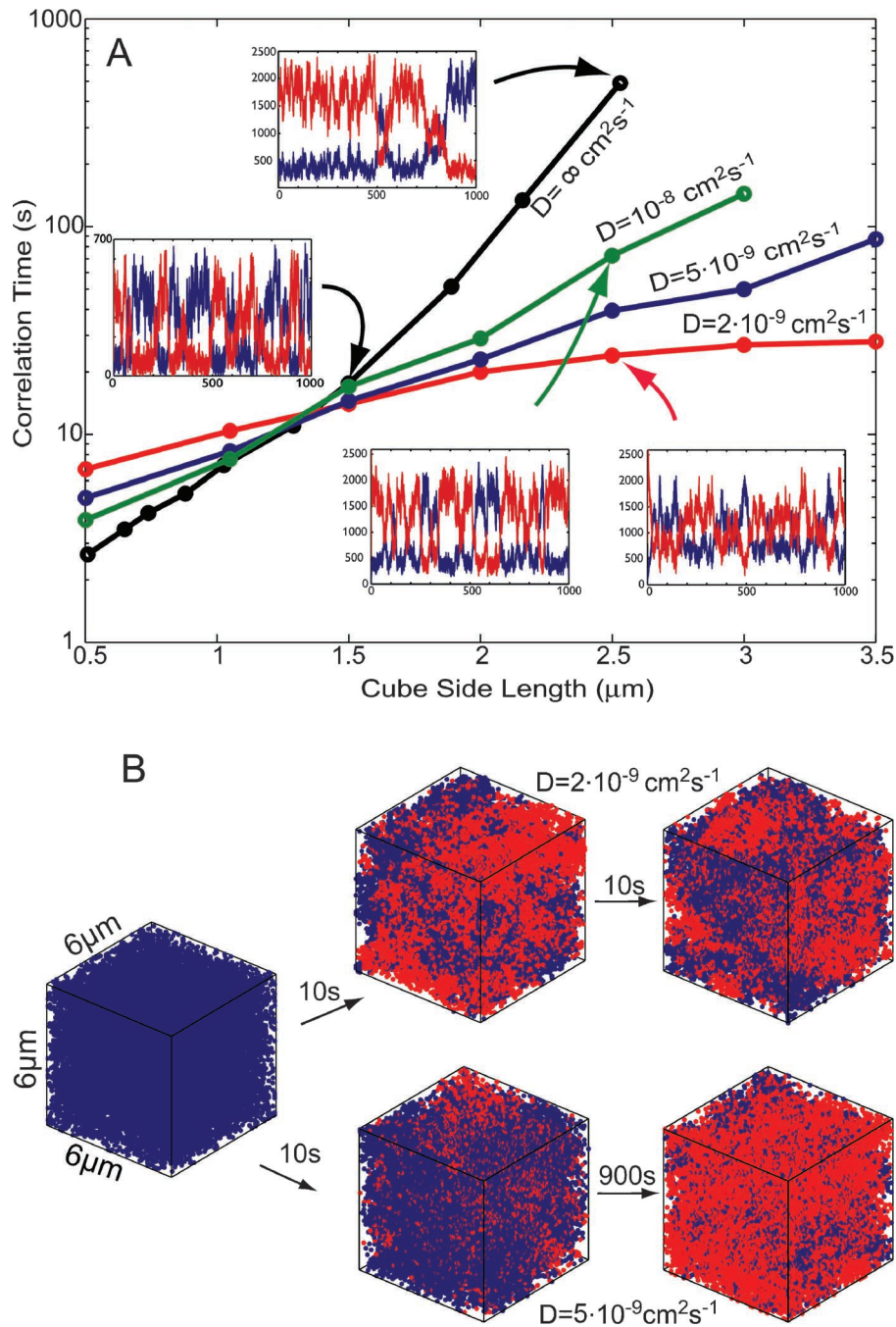


**Fig. 1** Reduction of escape time and domain separation

*a* Correlation times of A molecules is plotted for different volumes and diffusion constants. Example of time evolution of the total number of free A and B molecules are given for the points indicated by arrows

*b* Snap-shots of positions of A and B molecules some times after an initial condition with only B molecules. The volume is  $6 \times 6 \times 6 \mu\text{m}^3$  and  $D = 2 \cdot 10^{-9} \text{ cm}^2 \text{ s}^{-1}$  and  $D = 5 \cdot 10^{-9} \text{ cm}^2 \text{ s}^{-1}$ , respectively

why the bi-stability of the total system is almost lost in this case (Fig. 1a, insert from red line).

When  $D$  is  $5 \cdot 10^{-9} \text{ cm}^2 \text{ s}^{-1}$  there is no visible domain separation, and yet the system jumps between its attractors at a much faster rate than in the homogenous case with infinitely fast diffusion (Fig. 1b, compare also black and blue lines in Fig. 1a). Part of this increase in the frequency of transitions between the attractors can be ascribed to the reflecting boundaries. That is, close to the boundaries local fluctuations in molecule numbers away from their averages in the dominating phase are less restrained than at positions distal to the boundaries.

This can be seen as patches in the opposite phase near the corners in Fig. 1b.

To remove such boundary effects, so that the conditions for domain separation in arbitrarily large systems can be clarified, we have also simulated the behaviour of the system in the same volume as in Fig. 1b, but with periodic, rather than reflecting, boundary conditions. The system displays domain separation for  $D = 2 \cdot 10^{-9} \text{ cm}^2 \text{ s}^{-1}$  but not for  $D = 4 \cdot 10^{-9} \text{ cm}^2 \text{ s}^{-1}$  (see online supplementary Fig. 1). This implies that the red curve in Fig. 1a for  $D = 2 \cdot 10^{-9} \text{ cm}^2 \text{ s}^{-1}$  stays at the plateau also when  $L \rightarrow \infty$ , whereas the correlation times for the other curves go to infinity.

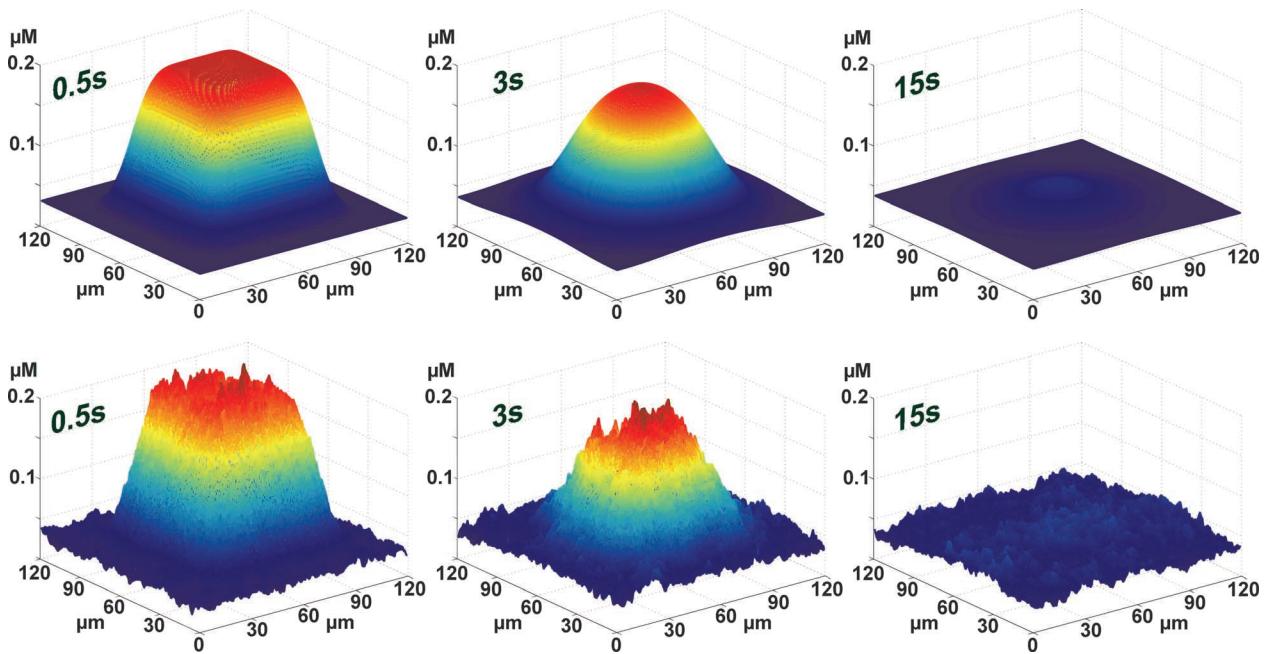


**Fig. 2** The macroscopic approximation in the limit of large  $D$

The time evolution of the concentrations of A molecules is illustrated by three snap-shots (0.5 s, 3 s and 15 s). The total spatial extension is  $120 \times 120 \times 0.6 \mu\text{m}$  and  $D = 5 \cdot 10^{-7} \text{cm}^2 \text{s}^{-1}$

a Solution of macroscopic reaction-diffusion partial differential equations  
b Realisation of the same process as described by RDME

### 2.3 The macroscopic reaction-diffusion equation and curvature of domain fronts

When this bi-stable system is inspected from a macroscopic perspective, the ordinary reaction diffusion equation (see online supplementary text A) allows for stable domains of opposite phases in 1D, but generally not in 2D or 3D. The reason is that a domain with a concave boundary will devour a neighbouring domain with its corresponding convex boundary, and only boundaries that lack curvature can be long-lived [25]. This is illustrated in Fig. 2, where the macroscopic reaction-diffusion equation is integrated for a flat geometry ( $120 \times 120 \times 0.6 \mu\text{m}$ ). The initial condition is that, in a square at the centre of the plane, the system is in the attractor with high concentration of A molecules, and in the remaining part of the volume, the system is in the other attractor (Fig. 2a). For comparison, we show a simulation based on the reaction diffusion master equation (Fig. 2b). Diffusion is in this case so fast that a large number of molecules are within diffusion range of each other. In this limit, the time evolution of the system is primarily governed by macroscopic laws, and the macroscopic and mesoscopic approaches lead to similar results (Fig. 2). With increasing time, the curvature is eliminated in that the initial square with high A molecule numbers transforms to a circle, which shrinks more and more and eventually disappears.

### 2.4 The rule for domain separation

What, then, is the rule that determines if a bi-stable system spontaneously separates into spatial domains of different phases? The possibility of domain separation depends, we suggest, on how two different average times react to changes in the total reaction volume  $V$ . The first is the correlation time ( $\tau_c$ ) for a homogenous helper system contained in  $V$  that is constructed in such a way that all chemical rate constants are identical with those in the real system. That is, the helper system is modelled as homogeneous but with diffusion limited rate constants as in the real system.

The correlation time of the helper system will therefore depend both on its volume and the diffusion constants (solid lines in Fig. 3). The second is the time ( $\tau_D$ ) to mix the molecules of the real system in  $V$  to homogeneity by diffusion. The mixing time,  $\tau_D$ , of the real system will depend on the shape of the volume and the rate of diffusion. We suggest that the rule for domain separation is that when  $\tau_c \leq \tau_D$  for at least one value of  $V$ , domain separation will occur in large systems, but otherwise not.

This type of behaviour is illustrated in Fig. 3 for a system contained in cubic 3D volume  $V$  with side length  $L = V^{1/3}$ . The solid lines are the correlation times ( $\tau_c$ ) for helper systems with reaction rates corresponding to  $D = 2 \cdot 10^{-9} \text{cm}^2 \text{s}^{-1}$  (black) and  $D = 5 \cdot 10^{-9} \text{cm}^2 \text{s}^{-1}$

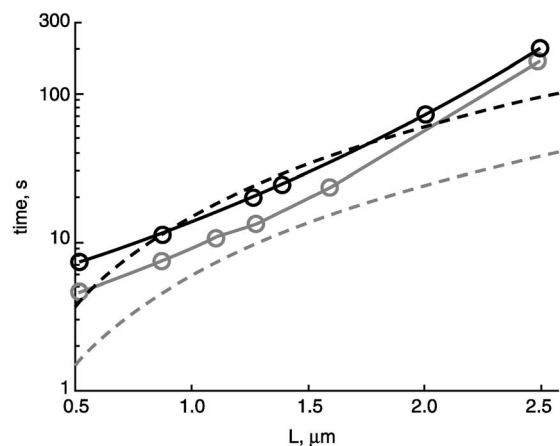


**Fig. 3** The correlation times for homogeneous helper systems of different volumes ( $L^3$ ) with kinetic parameters corresponding to  $D = 2 \cdot 10^{-9} \text{cm}^2 \text{s}^{-1}$  (black) and  $D = 5 \cdot 10^{-9} \text{cm}^2 \text{s}^{-1}$  (grey) are plotted as solid lines. These are compared to mixing times ( $3L^2/D$ ) of volumes of the same size (dashed). When, for some  $L$ , the curves intersect, the system displays domain separation in sufficiently large volumes, but not otherwise

(grey) for the real system. The mixing times ( $\tau_D$ ) required to keep the real systems homogenous by diffusion are proportional [10] to  $L^2/D$  with an empirically-estimated constant of proportionality (see online supplementary text C). The  $\tau_D$  values are plotted versus system volume (dashed lines) for  $D = 2 \cdot 10^{-9} \text{cm}^2 \text{s}^{-1}$  (black) and  $D = 5 \cdot 10^{-9} \text{cm}^2 \text{s}^{-1}$  (gray). When  $\tau_c > \tau_D$  for all  $L$ , the strong diffusion coupling between neighbouring regions prohibits domain separation. When, in contrast,  $\tau_c < \tau_D$  in some interval of  $L$ , domain separation is allowed, since the diffusion coupling between neighbouring regions is weak enough to allow for local attractor switches without rapid annihilation of the new phase by the surrounding opposite phase. In Fig. 3, the black curves for  $D = 2 \cdot 10^{-9} \text{cm}^2 \text{s}^{-1}$  intersect, and in accordance with the suggested rule, the corresponding spatially extended system displays domain separation (Fig. 1b). In contrast, the grey curves for  $D = 5 \cdot 10^{-9} \text{cm}^2 \text{s}^{-1}$  do not intersect and, also in accordance with the rule, there is no domain separation (Fig. 1b).

## 2.5 Diffusion in confined geometries

The cubic 3D volume with side length  $L = V^{1/3}$  has a short mixing time compared to a system where the same volume is distributed in a plane with thickness  $d \ll V^{1/3}$  and side length  $L = (V/d)^{1/2}$  (2D-like system) or in a tube with cross-section  $d^2$  and side length  $L = V/d^2$  (1D-like system). In the cubic case the mixing time is proportional to  $V^{2/3}/D$ , in the 2D-like case to  $V/(Dd)$ , and in the 1D-like case to  $V^2/(Dd^4)$ . Since  $V^{2/3} \ll V/d \ll V^2/d^4$ , it follows that when the same volume  $V$  is contained in a thin cylinder, like in a dendrite (1D-like system) [20], or if it is flattened between two membranes (2D-like system), the mixing time is much longer than when  $V$  is contained in a spherical or cubic volume (authentic 3D system). This implies that the occurrence of domain separation depends on the shape of

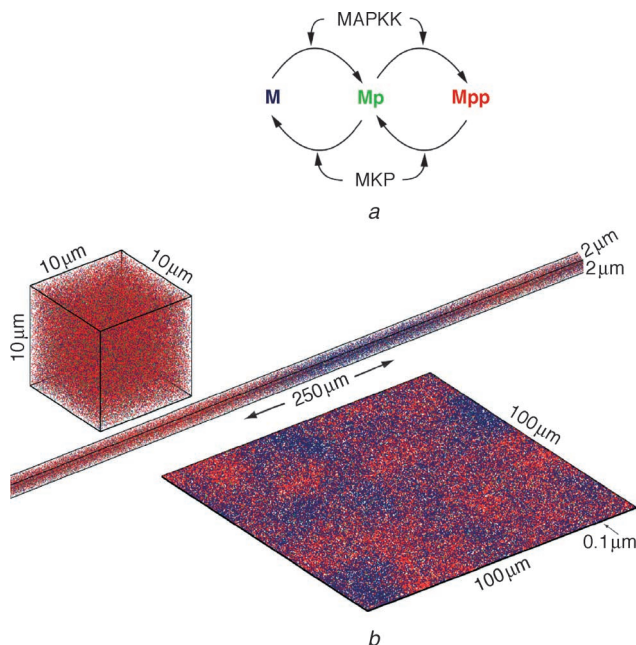


**Fig. 4** The same volume in different geometries

a A MAPK phosphorylation-dephosphorylation cycle with non-processive, distributed mechanisms for the kinase (MAPKK) and phosphatase (MKP) [34]. The scheme of elementary reactions and the parameters are given in the online supplementary text D  
b The system is simulated with  $D = 2 \cdot 10^{-8} \text{cm}^2 \text{s}^{-1}$  in a bounded volume of  $1000 \mu\text{m}^3$  distributed in different geometries. Only  $100 \mu\text{m}$  of the  $250 \mu\text{m}$  tube is shown

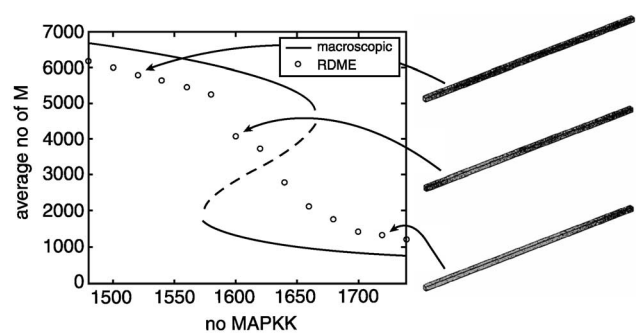


**Fig. 5** Loss of hysteresis in the MAPK system

X-axis: number of MAPKK molecules in a  $54 \mu\text{m}$  volume. Y-axis: stationary average number of unphosphorylated MAPK (M, black). In a macroscopic model the system displays classical hysteresis when the concentration of MAPKK increases and all other concentrations are kept constant (line). When the same system is simulated from the RDME in a  $1 \times 1 \times 54 \mu\text{m}$  volume with  $D = 2 \cdot 10^{-8} \text{cm}^2 \text{s}^{-1}$ , we see a gradual change in the number of M in the whole volume (circles). Snap-shots of the system state are indicated for some of the MAPKK concentrations

the system volume as well as on the diffusion constant and the kinetic parameters that determine  $\tau_j$ . Fig. 4 illustrates a case when a bi-stable MAPK phosphorylation-dephosphorylation cycle with non-processive, distributed kinase and phosphatase activities [34] displays domain separation in a tube or a flat geometry, but not in a cube. This system is described in more detail in the online supplementary text D.

## 2.6 Asymmetric bi-stable systems and hysteresis

So far, we have described symmetric systems where the attractors are equally stable. We will finally illustrate what happens if the MAPK system is made asymmetric by varying the concentration of MAPKK. Macroscopically, the MAPK will display hysteresis [2, 34] as demonstrated in Fig. 5 (line). This means that the system can reach different steady states depending on initial conditions and that the state is not reversible for all changes in MAPKK concentration. Likewise, when the conditions for spontaneous domain separation are not fulfilled, the system will display global hysteresis also in a mesoscopic model at a timescale that is faster than the escape rates from the attractors.

However, when spontaneous domain separation emerges, global hysteresis is lost. Instead, the average fraction of the volume that is in one attractor is changed when the concentration of MAPKK is varied over the bi-stable region, so that the average number of phosphorylated molecules in the whole volume changes gradually (Fig. 5). Locally, however, the systems may display hysteresis.

An equivalent loss of global hysteresis due to local fluctuations was recently demonstrated experimentally in inorganic surface catalysis [13].

## 3 Discussion

With the help of a new and highly efficient Monte Carlo algorithm adapted for the reaction-diffusion master equation we have analysed the stochastic behaviour of bi-stable systems in 3D. The results suggest general rules for when those systems separate into spatial domains of opposite phases. Spontaneous domain separation requires that a localised part of the system jumps from an attractor in phase to an attractor out of phase with the surroundings. For this to happen, the size of the part of the system that jumps out of phase must be big enough so that it is not invaded by

neighbouring molecules. At the same time, the size must be small enough so that the local escape from the original attractor does not take too long. It is only when there exists a local volume size for which invasion by diffusion takes a longer time than attractor escape, that spatial domains become sufficiently decoupled from their surroundings to allow for spontaneous domain separation. Accordingly, systems in tube-like or flat geometries display domain separation much more easily than do their spherical or cubic equivalents. Furthermore, geometric restrictions in small reaction volumes, like intracellular membrane structures, will reduce attractor escape times in localised areas which will strongly promote the emergence of spatial domains in opposite phases. This eliminates hysteresis in the total cell volume, meaning that absence of hysteresis cannot be used to infer lack of intrinsic bi-stability of an experimentally studied system [2].

Bi-stable switches in living cells may for their proper function depend on the existence of spatial domains in opposite phase. For instance, long-term potentiation (LTP) in post synaptic dendrites depends on a bi-stable system that separates into domains of opposite phase in a single cell [35, 36]. LTP is maybe partly mediated by phosphorylation of CaMKII following  $\text{Ca}^{2+}$  release [8, 37]. The phosphorylated state of CaMKII displays hysteresis, in that its activity remains high also after a reduction of the  $\text{Ca}^{2+}$  concentration [38]. These system properties are intriguing in light of the present results and lead to a number of questions: (i) how can CaMKII in adjacent synapses be in different activity states, when  $\text{Ca}^{2+}$  spreads through the dendrite? (ii) why is it that activated CaMKII in one synapse does not phosphorylate CaMKII in neighbouring synapses? (iii) how are spontaneous attractor escapes in local areas avoided? The answers are that the CaMKII system has evolved so that: (i) calcium signalling is isolated in tiny compartments (spines) protruding from the dendrites [39]; (ii) CaMKII can only be active when it is bound to protein scaffolds in the postsynaptic density [38]; (iii) CaMKII is a 12 subunit protein complex with about 30 phosphorylation sites, which makes it resilient to stochastic fluctuations [37].

In other cases, bi-stable control circuits must be in global attractors that extend throughout the whole intracellular space. Such examples are the tightly controlled cell fate decision circuits, which play essential roles in cell cycle regulation [40] and cell maturation [5]. These circuits must be designed so that domain separations do not occur and so that spontaneous attractor escape times are sufficiently long. This can be achieved by slow reaction kinetics in combination with unrestrained intracellular diffusion, ideally in a single, spherical compartment without nooks.

Spatially distributed protein phosphorylation cascades transmit signals from membrane-bound receptors to cytosolic targets [41]. These signal molecules are phosphorylated by membrane-bound kinases and dephosphorylated by cytosolic phosphatases, which can lead to concentration gradients and low signal strength in the target region [42]. It has been suggested that bi-stable signal systems could overcome this problem by their ability to maintain high signal strengths over long distances [43]. The proposed mechanism is attractive, but depends critically on the absence of local spontaneous state changes along communication channels from membrane receptor to target. This requires high signal molecule concentrations and free diffusion from signal source to signal target, unhindered by narrow passages or partially isolated compartments.

## 4 Acknowledgments

We thank Otto Berg, Upinder Bhalla, James Ferrell, Dan Gillespie, Malek Mansour, and Johan Paulsson for helpful comments on the manuscript. The work was supported by the National Graduate School of Scientific Computing and the Swedish Research Council.

## 5 References

- 1 Monod, J., and Jacob, F.: 'General conclusions: teleonomic mechanisms in intracellular metabolism, growth, and differentiation', *Cold Spring Harbour Symp. Quant. Biol.*, 1961, **26**, pp. 389–401
- 2 Ferrell, J.E., Jr.: 'Self-perpetuating states in signal transduction: positive feedback, double-negative feedback and bistability', *Current Opinion in Cell Biology*, 2002, **14**, pp. 140–148
- 3 Angeli, D., Ferrell, J.E., Jr., and Sontag, E.D.: 'Detection of multistability, bifurcations, and hysteresis in a large class of biological positive-feedback systems', *Proc. Natl. Acad. Sci. USA*, 2004, **101**, pp. 1822–1827
- 4 Tyson, J.J., Chen, K., and Novak, B.: 'Network dynamics and cell physiology', *Nat. Rev. Mol. Cell. Biol.*, 2001, **2**, pp. 908–916
- 5 Xiong, W., and Ferrell, J.E., Jr.: 'A positive-feedback-based bistable 'memory module' that governs a cell fate decision', *Nature*, 2003, **426**, pp. 460–465
- 6 Becskei, A., Seraphin, B., and Serrano, L.: 'Positive feedback in eukaryotic gene networks: cell differentiation by graded to binary response conversion', *Embo. J.*, 2001, **20**, pp. 2528–2535
- 7 Bhalla, U.S., Ram, P.T., and Iyengar, R.: 'MAP kinase phosphatase as a locus of flexibility in a mitogen-activated protein kinase signaling network', *Science*, 2002, **297**, pp. 1018–1023
- 8 Bhalla, U.S., and Iyengar, R.: 'Emergent properties of networks of biological signaling pathways', *Science*, 1999, **283**, pp. 381–387
- 9 Gardiner, C.: 'Handbook of stochastic methods' (Springer-Verlag, Berlin, 1985, 2nd edn.)
- 10 Van Kampen, N.G.: 'Stochastic processes in physics and chemistry' (Elsevier, Amsterdam, 1997, 2nd edn.)
- 11 Shapiro, L., and Losick, R.: 'Dynamic spatial regulation of the bacterial cell', *Cell*, 2000, **100**, pp. 89–98
- 12 Batada, N.N., Shepp, L.A., and Siegmund, D.O.: 'Stochastic model of protein-protein interaction: why signaling proteins need to be colocalized', *Proc. Natl. Acad. Sci. USA*, 2004, **101**, pp. 6445–6449
- 13 Johannek, V., Laurin, M., Grant, A.W., Kasemo, B., Henry, C.R., and Libuda, J.: 'Fluctuations and bistabilities on catalyst nanoparticles', *Science*, 2004, **304**, pp. 1639–1644
- 14 Paulsson, J.: 'Summing up the noise in gene networks', *Nature*, 2004, **427**, pp. 415–418
- 15 Korobkova, E., Emonet, T., Vilar, J.M., Shimizu, T.S., and Cluzel, P.: 'From molecular noise to behavioural variability in a single bacterium', *Nature*, 2004, **428**, pp. 574–578
- 16 McQuarrie, D.A.: 'Stochastic approach to chemical kinetics', *J. Appl. Probab.*, 1967, **4**, pp. 413–478
- 17 Elowitz, M.B., Surette, M.G., Wolf, P.E., Stock, J.B., and Leibler, S.: 'Protein mobility in the cytoplasm of Escherichia coli', *J. Bacteriol.*, 1999, **181**, pp. 197–203
- 18 Howard, M., and Rutenberg, A.D.: 'Pattern formation inside bacteria: fluctuations due to the low copy number of proteins', *Phys. Rev. Lett.*, 2003, **90**, p. 128102
- 19 Turing, A.M.: 'The chemical basis of morphogenesis', *Philos. Trans. R. Soc. Lond.*, 1952, **237**, pp. 37–72
- 20 Finch, E.A., and Augustine, G.J.: 'Local calcium signaling by inositol-1,4,5-trisphosphate in Purkinje cell dendrites', *Nature*, 1998, **396**, pp. 753–756
- 21 Thar, R., and Kuhl, M.: 'Bacteria are not too small for spatial sensing of chemical gradients: an experimental evidence', *Proc. Natl. Acad. Sci. USA*, 2003, **100**, pp. 5748–5753
- 22 Nicolis, G., and Prigogine, I.: 'Self-organization in nonequilibrium systems' (John Wiley, New York, 1977)
- 23 Baras, F., and Mansour, M.M.: 'Microscopic simulation of chemical instabilities', *Adv. Chem. Phys.*, 1997, **100**, pp. 393–475
- 24 Gorecki, J., Kawaczynski, A.L., and Nowakowski, B.: 'Master equation and molecular dynamics simulations of spatiotemporal effects in a bistable chemical system', *J. Phys. Chem. A*, 1999, **103**, pp. 3200–3209
- 25 Mikhailov, A.: 'Foundations of synergetics I', in Haken, H. (Ed.): (Springer Verlag, Berlin, 1990)
- 26 Meerson, B.: 'Domain stability, competition, growth, and selection in globally constrained bistable systems', *Phys. Rev. E*, 1996, **53**, pp. 3491–3494
- 27 Gillespie, D.: 'A general method for numerically simulating the stochastic time evolution of coupled chemical reactions', *J. Comput. Phys.*, 1976, **22**, pp. 403–434
- 28 Malek-Mansour, M., and Houard, J.: 'A new approximation scheme for the study of fluctuations in nonuniform nonequilibrium systems', *Phys. Lett. A*, 1979, **70**, pp. 366–368
- 29 And er, M., Beltrao, P., Di Ventura, B., Ferkinghoff-Borg, J., Foglierini, M., Kaplan, A., Lemerle, C., Tomas-Oliveira, I., and Serrano, L.: 'SmartCell: a framework to simulate cellular processes that

- combines stochastic approximation with diffusion and localisation: analysis of simple gene networks', *Systems Biology*, 2004, **1**
- 30 Andr , M.: 'SmartCell - a general framework for whole cell modelling and simulation', *UPTEC X 02 021*, 2002, [http://www.ibg.uu.se/upload/2002-11-18\\_162646\\_535/Maria\\_A.pdf](http://www.ibg.uu.se/upload/2002-11-18_162646_535/Maria_A.pdf)
  - 31 Kaplan, A.: 'On whole-cell modelling and simulation', *UPTEC X 01 044*, ISSN 1401-2138 2001, [http://www.ibg.uu.se/upload/2002-07-10\\_225930\\_995/01044.pdf](http://www.ibg.uu.se/upload/2002-07-10_225930_995/01044.pdf)
  - 32 Gibson, M., and Bruck, J.: 'Efficient exact stochastic simulation of chemical systems with many species and channels', *J Phys. Chem. A*, 2000, **104**, pp. 1876–1889
  - 33 Berg, O.G.: 'On diffusion-controlled dissociation', *Chem. Phys.*, 1978, **31**, pp. 47–57
  - 34 Markevich, N.I., Hoek, J.B., and Kholodenko, B.N.: 'Signaling switches and bistability arising from multisite phosphorylation in protein kinase cascades', *J Cell. Biol.*, 2004, **164**, pp. 353–359
  - 35 Koch, C.: 'Biophysics of computation' (Oxford University Press, New York, 1999)
  - 36 Lisman, J.E.: 'A mechanism for memory storage insensitive to molecular turnover: a bistable autophosphorylating kinase', *Proc. Natl. Acad. Sci. USA*, 1985, **82**, pp. 3055–3057
  - 37 Lisman, J.E., and Goldring, M.A.: 'Feasibility of long-term storage of graded information by the Ca<sup>2+</sup>/calmodulin-dependent protein kinase molecules of the postsynaptic density', *Proc. Natl. Acad. Sci. USA*, 1988, **85**, pp. 5320–5324
  - 38 Lisman, J.E., and Zhabotinsky, A.M.: 'A model of synaptic memory: a CaMKII/PP1 switch that potentiates transmission by organizing an AMPA receptor anchoring assembly', *Neuron*, 2001, **31**, pp. 191–201
  - 39 Augustine, G.J., Santamaria, F., and Tanaka, K.: 'Local calcium signaling in neurons', *Neuron*, 2003, **40**, pp. 331–346
  - 40 Sha, W., Moore, J., Chen, K., Lassaletta, A.D., Yi, C.S., Tyson, J.J., and Sible, J.C.: 'Hysteresis drives cell-cycle transitions in *Xenopus laevis* egg extracts', *Proc. Natl. Acad. Sci. USA*, 2003, **100**, pp. 975–980
  - 41 Chang, L., and Karin, M.: 'Mammalian MAP kinase signalling cascades', *Nature*, 2001, **410**, pp. 37–40
  - 42 Kholodenko, B.N.: 'MAP kinase cascade signaling and endocytic trafficking: a marriage of convenience?', *Trends Cell. Biol.*, 2002, **12**, pp. 173–177
  - 43 Kholodenko, B.N.: 'Four-dimensional organization of protein kinase signaling cascades: the roles of diffusion, endocytosis and molecular motors', *J. Exp. Biol.*, 2003, **206**, pp. 2073–2082

# Supplementary Methods: The Next Subvolume Method

The algorithm described below generates exact realizations of the Markov process described by the reaction diffusion master equation. An early version of the algorithm was presented at the SPIE conference on fluctuations and noise in biological, biophysical and biomedical systems in Santa Fe 2003 [1].

**Short explanation for those who are familiar with the “next reaction method”[2] and the “direct method” [3]** The reaction and diffusion rates in a single subvolume are given by the numbers of the different types of molecules that it contains. The time for the next event in each subvolume, *i.e.* a chemical reaction or a diffusion jump out from it, can thus be calculated individually by the *direct method*. The question is in which subvolume an event occurs first. To identify the subvolume where the first event occurs, we use the *next reaction method*. A single event can change the state of only one or two subvolume(s). If the event was a chemical reaction, the next event time has to be up-dated only for the subvolume where it occurred. If the event was a diffusion jump out, next event times have to be up-dated for the subvolume from which the jump occurred and for the subvolume to which the molecule jumped.

## The algorithm

### Initialization

1. Generate a *connectivity matrix* (Fig. M2) that describes the geometry of the system.
2. Distribute the initial numbers of molecules between the subvolumes and store in the *configuration matrix*. This can be done randomly or according to any initial distribution.
3. Calculate the sum of reaction rates  $r_i$  for each subvolume  $i$  and store in the *rate matrix*. The reaction rates are calculated for the size  $\Delta$  of the subvolume, as in the reaction-diffusion master equation.
4. Calculate the sum of diffusion rates for each subvolume,  $s_i = n_i \sum_{j=1}^M d_j X_j^i$ , where  $d_j = D_j / \ell^2$  is the diffusion rate constant for species  $j$ .  $X_j^i$  is the number of molecules of species  $j$  in subvolume  $i$ .  $M$  is the number of species.  $n_i$  is the number of directions in which the molecules can diffuse. Store  $s_i$  in the *rate matrix*.
5. For each subvolume  $i$ : (a.) sum  $r_i + s_i$ , (b.) generate a random number, *rand*, uniformly distributed between 0 and 1 and (c.) calculate the first event time for each subvolume as  $\tau_i = -\ln(\text{rand}) / (r_i + s_i)$ .
6. Make an initial ordering of the subvolumes according to their next event times. The subvolumes are kept sorted in a binary tree (an *event queue*, see below) so that the subvolume for which the event occurs first is on the top and all branches have increasing event times.

### Iterations

7. Assume that  $\lambda$  is the subvolume in which the next event occurs at time  $t = \tau_\lambda$  according to the top element of the event queue. Generate a random number *rand* uniformly distributed between 0 and 1, choose a chemical reaction if  $\text{rand} < r_\lambda / (r_\lambda + s_\lambda)$  and otherwise a diffusion jump.
8. Reaction event:
  - a. Rescale *rand* from (7.) linearly to [0,1] to determine which reaction occurred as in the direct method.
  - b. Update the state of the subvolume  $\lambda$  in the configuration matrix according to the state changes by reaction.
  - c. Recalculate the sum  $r_\lambda + s_\lambda$  for the subvolume  $\lambda$ , generate a new random number and calculate the time of the next event as  $t_\lambda = -\ln(\text{rand}) / (r_\lambda + s_\lambda) + t$ .
  - d. Insert the active subvolume's new event time in the event queue and order the queue (see below).
9. Diffusion event:
  - a. Rescale *rand* from (7.) linearly to [0,1] to determine which type of molecule that diffused away. The diffusion intensities are given by the numbers of the different types of molecules weighted by their diffusion rate constants.
  - b. The direction of the diffusion event is chosen by randomly selecting a column in the connectivity matrix. This can be done by rescaling the random number used in 9a (again).
  - c. Update the states of both subvolume  $\lambda$  and its neighbor,  $\gamma$ , that got an additional molecule.
  - d. Recalculate the sums  $r_\lambda + s_\lambda$  and  $r_\gamma + s_\gamma$ , sample the time to the next event in the subvolumes as in 8c.
  - e. Insert the subvolumes' new event times in the event queue and order the queue (see below).
10. Return to 7. for the next iteration.

## Further Improvements

The algorithm can be modified in a number of ways for particular systems depending on tradeoffs between memory usage and speed. E.g., it is possible to store all reaction rates for each subvolume, such that they do not have to be recalculated in 8a. Alternatively, it is possible to sample the reaction or diffusion event that will occur next simultaneously with the event time in 8c and 9d. The draw-back is that a random number is wasted if a molecule diffuses into the subvolume before its event time.

Another possible improvement is to reuse the event time for the subvolume where the state changed because a molecule diffused into it in step 9d. Gibson and Bruck [2] proved that the old event time can be reused, without sampling a new random number. In the procedure above it is re-sampled every time. Let  $\gamma$  be the subvolume for which the state has changed because a molecule diffused into it, so that its total rate changed from  $r_{\gamma,old} + s_{\gamma,old}$  to  $r_{\gamma,new} + s_{\gamma,new}$ . The next event time  $\tau_{new}$  can be recalculated as  $\tau_{new} = (r_{\gamma,old} + s_{\gamma,old}) / (r_{\gamma,new} + s_{\gamma,new}) (\tau_{old} - t) + t$ , instead of as  $-\ln(rand) / (r_{\gamma,new} + s_{\gamma,new}) + t$ , which would require an additional random number. See [2] for more details. This improvement has not been used in the present simulations.

For reaction systems where only a few of the reaction rates in a subvolume are affected by a state change it may be advantageous to implement the Next Reaction Method [2] to sample the reaction or diffusion event in each subvolume. The procedures described above use the Direct Method [3] at the level of subvolumes.

Blue et al. [4] and Wong and Easton [5] have earlier described another binary tree search algorithm for exact Monte Carlo simulation of the master equation [3, 6], which could possibly be useful also for reaction diffusion problems as suggested by Breuer et al. [7].

In a direct application of the Next Reaction Method, the event times are calculated for each event, rather than for each subvolume. Further all events are ordered in the propriety queue and the geometry of the system is implicitly built into the dependency graph, that is used to keep track of how many and which event times that should be recalculated after each event. When the number of subvolumes is large, the Next Subvolume Method (NSM) is more efficient than a direct application of the Next Reaction Method (NRM) to the RDME. The major reason is that the NRM requires an exceptionally large dependency graph to describe which and how many event times that need to be recalculated after each event. The size of this data structure would cause memory problems. Furthermore, in the NSM the number of elements in the priority queue is equal to the number of subvolumes,  $C$ , and the queue is reordered twice for each diffusion event. In the NRM the number of elements in the priority queue is approximately  $C(6N+R)$ , where  $N$  is the number of diffusing species and  $R$  is the number of different reactions in a subvolume. This larger queue must at average be reordered more than 12 times for each diffusion event.

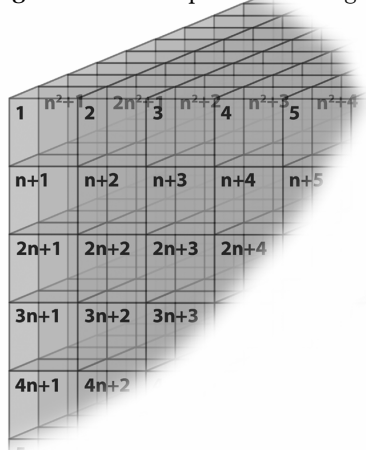
## The event queue

The event queue allows identification of the subvolume in which a next reaction will occur without searching through scheduled reaction times for all subvolumes or keeping them all sorted, which would take a time proportional to the number of subvolumes ( $N$ ). The event queue data structure is a binary tree, in which each element contains the index of a subvolume and the time for its next event, provided that no molecule enters by diffusion. The queue is ordered so that an element with an earlier event time is higher up on a branch. When the event time for a subvolume is changed, its position is changed up or down in the tree. When it gets an earlier time it changes place with the cell above until the branch is ordered. When it gets a later time it changes place with the subvolume below with the earliest scheduled time until the branch is ordered. Therefore it will take maximally  $\log_2(N)$  swaps per iteration to keep the queue sorted. The branched structure is conveniently stored in a *queue array*, where each row is an element of the queue. The elements above element  $k$  in the queue are thus placed on a row with index “ $(k/2)$  truncated to an integer” and the elements below have the row indices  $2k$  and  $2k+1$ . Each element in the queue is listed with a reference from an array sorted on subvolume number. This array is necessary to identify the element in the queue that corresponds to the neighbor of the active subvolume.

### The connectivity matrix and boundary conditions

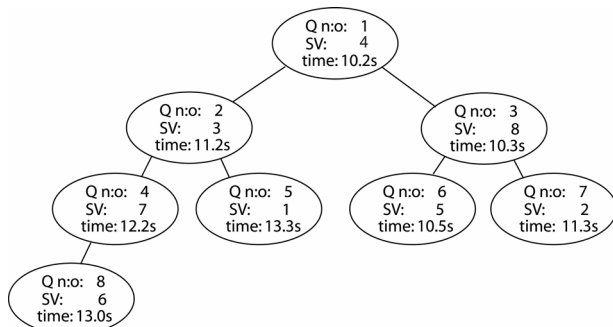
In order to rapidly find the subvolume number of a neighboring subvolume we generate a look-up table; the connectivity matrix. Each row in the matrix corresponds to one subvolume and the subvolume indices are conveniently chosen as the row numbers. The subvolume indices for each of the six neighbors are stored in different columns. This determines the geometry of the system. Using the connectivity matrix, one obtains the index for the subvolume where a molecule diffuses by randomly choosing a column in the row corresponding to the active subvolume. Periodic or closed boundaries are simply created by assigning the appropriate neighbors. For closed boundaries diffusion can be directed back to the same subvolume by assigning the row index to some element in the row.

Fig. M1 An example of indexing  $n^3$  cells.



$i$	$n1$	$n2$	$n3$	$n4$	$n5$	$n6$	#A	#B	#C	$r_i [s^{-1}]$	$s_i [s^{-1}]$	$r_i+s_i [s^{-1}]$	Q
1	2	1	3	1	5	1	10	2	0	2.2	10	12.2	5
2	2	1	4	2	6	2	9	1	3	4.2	11.3	15.5	7
3	4	3	3	1	7	3	5	0	2	2.3	5.4	7.3	2
4	4	3	4	2	8	4	7	1	1	1.4	6.4	7.8	1
5	6	5	7	5	5	1	4	0	2	0.4	4.3	4.7	6
6	6	5	8	6	6	2	7	1	3	0.5	10.3	10.8	9
7	8	7	7	5	7	3	8	2	4	1.0	13.3	14.3	4
8	8	7	8	6	8	4	5	0	2	5.3	5.4	10.7	3

Connectivity matrix      Configuration      Rate matrix      Q-array



Event Queue

Position in Queue (Q)	Subvolume (SV)	$\tau_i$ (s)
1	4	10.2
2	3	11.2
3	8	10.3
4	7	12.2
5	1	13.3
6	5	10.5
7	2	11.3
8	6	13.0

Fig. M2. Data structures The structures within solid borders are arrays used in the algorithm. The *connectivity matrix* ( $N \times 6$ ) stores the neighboring subvolumes' indices ( $n1-n6$ ) for each subvolume (*rows*). This defines the geometry and boundary conditions for the system. The *configuration matrix* ( $N \times M$ ) stores the present number of molecules of each species in each cell. The *rate matrix* ( $N \times 3$ ) stores the sum of reaction rate constants ( $r$ ) and the sum of diffusion rate constants ( $d$ ). The Q array keeps a reference to the subvolume's position in the *event queue*. In the *event queue* the subvolumes are ordered such that the one with the first scheduled event time ( $t$ ) is at the top and each branch is sorted with increasing event times.

## Justification

At time  $t$  the probability that any event will occur in subvolume  $m$  between  $t + \tau$  and  $t + \tau + \Delta\tau$  and that no event occurs in any subvolume before time  $\tau$  is

$$\Delta\tau P(m, \tau) = \Delta\tau \sum_i r_i^m \times \prod_{j,n} \exp(-r_j^n \tau) = \Delta\tau \sum_i r_i^m \times \exp\left(-\sum_n \sum_j r_j^n \tau\right). \quad (1)$$

Here,  $\Delta\tau r_i^m$  is the probability that event  $i$  in subvolume  $m$  will occur during the short time  $\Delta\tau$ .  $\Delta\tau \sum_i r_i^m$  is the probability that any event in subvolume  $m$  will occur during the short time  $\Delta\tau$ .  $\exp(-r_j^n \tau)$  is the probability that reaction  $j$  in subvolume  $n$  has not occurred during time  $\tau$ .  $\prod_{j,n} \exp(-r_j^n \tau)$  is the probability that no event has occurred in any subvolume during time  $\tau$ .

If the total rate of events in a subvolume  $m$   $\sum_i r_i^m = a_m$ , Eq. (1) reduces to

$$\Delta\tau P(m, \tau) = \Delta\tau a_m \times \exp\left(-\sum_n a_n \tau\right) \quad (2)$$

This expression for the probability that the next event occurs in subvolume  $m$  between  $t + \tau$  and  $t + \tau + \Delta\tau$  is equivalent to the expression sampled with the Next Reaction Method [2]. The Next Reactions Method can therefore be used to determine in which sub volume the next event will occur as well as the time of this event.

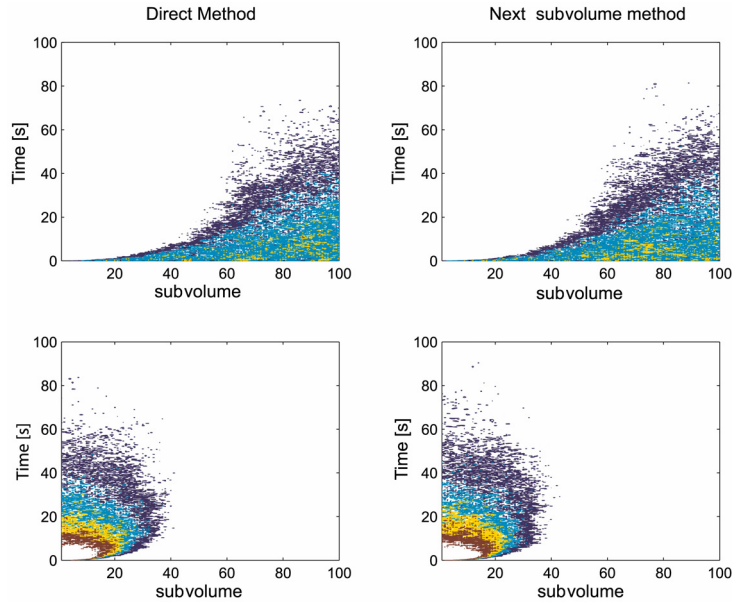
Next, we sample which event actually occurred in proportion to the rates,  $r_i^m$ , of the events in subvolume  $m$ , i.e. the occurrence of event  $i$  in subvolume  $m$  between  $t + \tau$  and  $t + \tau + \Delta\tau$  is sampled with probability

$$\Delta\tau P(i, m, \tau) = \Delta\tau P(i|m)P(m, \tau) = \Delta\tau \left(\frac{r_i^m}{a_m}\right) a_m \times \exp\left(-\sum_n a_n \tau\right) = \Delta\tau r_i^m \times \exp\left(-\sum_n a_n \tau\right). \quad (3)$$

It can now be seen that Eq. (3) is equivalent to the probability distribution sampled by Gillespie's direct method [3]. This means that the method can be applied also to spatially homogenous reaction networks with a large number of sparsely connected sub-networks, where the sub-networks have high internal connectivity.

### Fig M3. Comparison between the Next Subvolume Method and the Direct Method.

To illustrate in a concrete case the equivalence of the algorithm to previous exact methods for simulation of the Markov process described by the master equation, we have simulated the reaction  $A + B \xrightarrow{k_1} \emptyset$  with the Direct Method [3] and the Next Subvolume Method [this work]. The volume is  $0.4\mu\text{m} \times 0.4\mu\text{m} \times 40\mu\text{m}$  and it is divided into  $1 \times 1 \times 100$  subvolumes.  $k_1 = 10^8 \text{ M}^{-1}\text{s}^{-1}$  and  $D = 5 \cdot 10^{-8} \text{ cm}^2\text{s}^{-1}$ . Initially, 1000 A molecules are evenly distributed over the subvolumes, whereas 1000 B molecules all are located in one of the outermost subvolumes. As time goes by all molecules are eventually annihilated. The figure shows contour plots for A molecules at the top and B molecules at the bottom. The contours corresponds to 5, 10, 15, 20 molecules.



## Supplementary References

1. Elf, J., Doncic, A., and Ehrenberg, M.: Mesoscopic reaction-diffusion in intracellular signaling, *SPIE: Fluctuations and noise in Biological, Biophysical and Biomedical Systems*, 2003, **5110**:114-124.
2. Gibson, M. and Bruck, J.: Efficient exact stochastic simulation of chemical systems with many species and channels, *J Phys. Chem. A*, 2000, **104**:1876-1889.
3. Gillespie, D.: A general method for numerically simulating the stochastic time evolution of coupled chemical reactions, *J. Comp. Phys.*, 1976, **22**:403-434.
4. Blue, J.L., Beichl, I.I., and Sullivan, F.: Faster Monte Carlo simulations, *Physical Review. E. Statistical Physics, Plasmas, Fluids, and Related Interdisciplinary Topics*, 1995, **51**:R867-R868.
5. Wong, C.K. and Eatson, M.C.: *SIAM J. Comput.*, 1980, **9**:111.
6. Bortz, A., Kalos, M., and Lebowitz, J.: A New Algorithm for Monte Carlo Simulation of Ising Spin Systems, *J. Comp. Phys.*, 1975, **17**:10-8.
7. Breuer, H.P., Huber, W., and Petruccione, F.: Fast Monte Carlo algorithm for nonequilibrium systems, *Physical Review. E. Statistical Physics, Plasmas, Fluids, and Related Interdisciplinary Topics*, 1996, **53**:4232-4235.

# Supplementary Text

## A. Equations for the double negative feedback scheme

### The macroscopic reaction-diffusion equations

The macroscopic reaction-diffusion equations for the scheme in the main text are

$$\begin{aligned}\frac{da(r,t)}{dt} &= k_1 \cdot e_A + k_d \cdot a_2 e_B + k_d \cdot a e_B - k_a \cdot a \cdot e_B - k_4 \cdot a + D\nabla^2 a \\ \frac{db(r,t)}{dt} &= k_1 \cdot e_B + k_d \cdot b_2 e_A + k_d \cdot b e_A - k_a \cdot b \cdot e_A - k_4 \cdot b + D\nabla^2 b \\ \frac{de_B(r,t)}{dt} &= k_d \cdot a e_B - k_a \cdot a \cdot e_B + D\nabla^2 e_B \\ \frac{dae_B(r,t)}{dt} &= k_a \cdot a \cdot e_B - k_d \cdot a e_B + k_d \cdot a_2 e_B - k_a \cdot a \cdot a e_B + D\nabla^2 a e_B \\ \frac{da_2 e_B(r,t)}{dt} &= k_a \cdot a \cdot a e_B - k_d \cdot a_2 e_B + D\nabla^2 a_2 e_B \\ \frac{de_A(r,t)}{dt} &= k_d \cdot a e_A - k_a \cdot b \cdot e_A + D\nabla^2 e_A \\ \frac{dbe_A(r,t)}{dt} &= b \cdot e_A - k_d \cdot b e_A + k_d \cdot b_2 e_A - k_a \cdot b \cdot b e_A + D\nabla^2 a e_A \\ \frac{db_2 e_B(r,t)}{dt} &= k_a \cdot b \cdot b e_A - k_d \cdot b_2 e_A + D\nabla^2 b_2 e_A\end{aligned}$$

Each lower case letter on the left side in this equation system is the concentration of a species named by the corresponding capital letter.

### The reaction-diffusion master equation

The reaction-diffusion master equation for the double negative feedback scheme in the main text is

$$\begin{aligned}\frac{dP(\{A_\lambda, B_\lambda, C_\lambda, D_\lambda, E_\lambda, F_\lambda, G_\lambda, H_\lambda\}, t)}{dt} = & \\ \sum_\lambda \left[ C_\lambda k_1 (\mathbb{E}_\lambda^{-A} - 1) P + D_\lambda k_1 (\mathbb{E}_\lambda^{-B} - 1) P + \right. & \\ \Delta^{-1} k_a (\mathbb{E}_\lambda^{B,C,-E} - 1) B_\lambda C_\lambda P + \Delta^{-1} k_a (\mathbb{E}_\lambda^{A,D,-F} - 1) A_\lambda D_\lambda P + & \\ \Delta^{-1} k_a (\mathbb{E}_\lambda^{B,E,-G} - 1) B_\lambda E_\lambda P + \Delta^{-1} k_a (\mathbb{E}_\lambda^{A,F,-H} - 1) A_\lambda F_\lambda P + & \\ k_d (\mathbb{E}_\lambda^{-B,-C,E} - 1) E_\lambda P + k_d (\mathbb{E}_\lambda^{-A,-D,F} - 1) F_\lambda P + & \\ k_d (\mathbb{E}_\lambda^{-B,-E,G} - 1) G_\lambda P + k_d (\mathbb{E}_\lambda^{-A,-F,H} - 1) H_\lambda P + & \\ k_4 (\mathbb{E}_\lambda^A - 1) A_\lambda P + k_4 (\mathbb{E}_\lambda^B - 1) B_\lambda P \left. \right] + & \\ \sum_\lambda \sum_{\gamma \neq \lambda} \sum_{X=\{A \dots H\}} (\mathbb{E}_\gamma^X \mathbb{E}_\lambda^{-X} - 1) d_{\lambda\gamma}^X X_\lambda P &\end{aligned}$$

The numbers of A, B, E<sub>A</sub>, E<sub>B</sub>, E<sub>A</sub>B, E<sub>B</sub>A, E<sub>A</sub>B<sub>2</sub> and E<sub>B</sub>A<sub>2</sub> molecules are designated A, B, C, D, E, F, G and H, respectively. The indices λ or γ specify sub-volumes, with volume Δ = ℓ<sup>3</sup>, so that e.g. C<sub>λ</sub> is the number of E<sub>A</sub> molecules in sub-volume λ. The step operator,  $\mathbb{E}$ , is defined so that  $\mathbb{E}_\lambda^{A,-B} f(\dots A_\lambda, \dots, B_\lambda \dots) = f(\dots A_\lambda + 1, \dots, B_\lambda - 1 \dots)$ .  $d_{\lambda\gamma}^X$  is a first order rate constant that describes the diffusion jump of a molecule of type X from sub-volume λ to sub-volume γ.  $d_{\lambda\gamma}^X = d_{\gamma\lambda}^X = D/\ell^2$  for neighboring sub-volumes and  $d_{\lambda\gamma}^X = d_{\gamma\lambda}^X = 0$  otherwise.

## Criteria for selecting sub-volume size

The side length  $\ell$  of the cubic sub-volumes was chosen to satisfy the inequalities

$$R^2 \ll \ell^2 \ll 6D\tau_{\min}$$

The first criterion is that  $\ell$  must be much larger than any reaction radius  $R$ , so that dissociation events can be properly defined within sub-volumes. The second criterion is that the time  $\ell^2/6D$  for any molecule to leave a sub-volume must be much smaller than the shortest life time  $\tau_{\min}$  among the molecular species, so that all molecules are homogeneously distributed within the sub-volumes.

The 3D simulations were performed with  $\ell=0.1\mu\text{m}$ , which is twenty times larger than the reaction radius  $R=5\text{nm}$ . In the case of the smallest diffusion constant ( $D=2\cdot 10^{-9}\text{cm}^2\text{s}^{-1}$ ),  $\ell^2/6D$  is  $0.008\text{ s}$ , which is much shorter than the chemical life times of all molecules:

$$\text{A and B } (k_4 + k_a[E_{\text{tot}}])^{-1} \approx 0.162\text{ s } (\tau_{\min})$$

$$E_A \text{ and } E_B (k_a[X^*])^{-1} \approx 0.358\text{ s}$$

$$E_A B \text{ and } E_B A (k_a[X^*] + k_d)^{-1} \approx 0.256\text{ s}$$

$$E_A B_2 \text{ and } E_B A_2 (k_d)^{-1} \approx 0.903\text{ s}$$

$[X^*]$  is the concentration of the dominant product (A or B) in an attractor.

## Variation of the size and number of sub-volumes

Domain separation and other properties of the system remain the same when the sub-volume size increases from  $\Delta=\ell^3=0.1^3\mu\text{m}^3$  (Fig. N1A) to  $\Delta=\ell^3=0.2^3\mu\text{m}^3$  (Fig. N1B). When periodic boundary conditions are used, an increase in the total system volume does not affect domain separation (Compare Figs N1A and N1C).

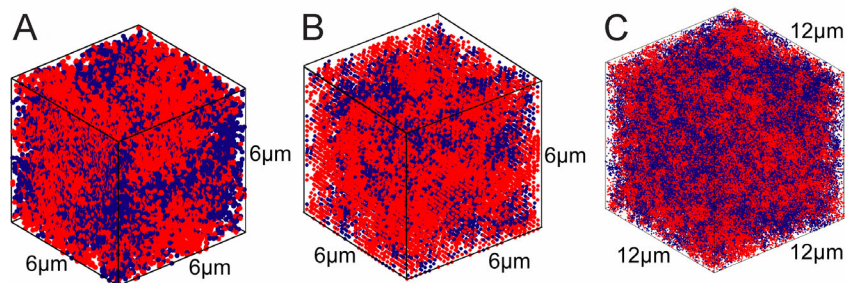


**Fig. N1.**

A.  $D=2\cdot 10^{-9}\text{ cm}^2\text{s}^{-1}$ ,  $60\times 60\times 60=216\ 000$  sub-volumes with  $\ell=0.1\mu\text{m}$ , periodic boundaries.

B.  $D=2\cdot 10^{-9}\text{ cm}^2\text{s}^{-1}$ ,  $30\times 30\times 30=27\ 000$  sub-volumes with  $\ell=0.2\mu\text{m}$ , periodic boundaries.

C.  $D=2\cdot 10^{-9}\text{ cm}^2\text{s}^{-1}$ ,  $120\times 120\times 120=1\ 728\ 000$  sub-volumes with  $\ell=0.1\mu\text{m}$ , periodic boundaries.

Domain separation and other properties of the system remain the same when the sub-volume size decreases from  $\Delta=\ell^3=0.3^3\mu\text{m}^3$  (Fig. N2A) to  $\Delta=\ell^3=0.1^3\mu\text{m}^3$  (Fig. N2B). In N2A the number of sub-volumes is  $316\times 316\times 1=99856$  and in N2B the number of sub-volumes is  $1000\times 1000\times 3=3000000$ .

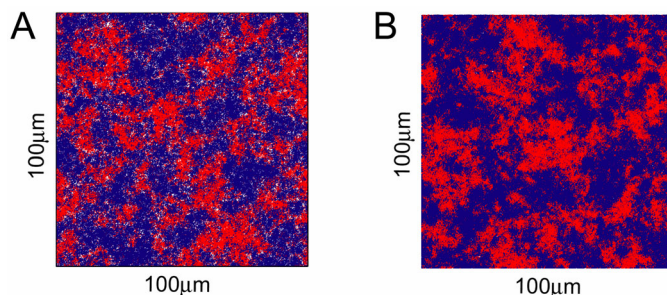


**Fig. N2.**

A.  $D=1\cdot 10^{-8}\text{ cm}^2\text{s}^{-1}$ ,  $330\times 330\times 1$  sub-volumes with  $\ell=0.3\mu\text{m}$  Periodic boundaries.

B.  $D=1\cdot 10^{-8}\text{ cm}^2\text{s}^{-1}$ ,  $1000\times 1000\times 3$  sub-volumes with  $\ell=0.1\mu\text{m}$  Periodic boundaries.

## B. How association and dissociation rate constants depend on the diffusion constant

When the diffusion constant is varied, the association and dissociation rate constants of partially diffusion controlled reactions change as well [1-3]. For the binding reaction  $A + B \xrightarrow{k_a} C$  of spherical A and B molecules the association rate constant is given by

$$k_a = \frac{4\pi D_{AB} R k N_A}{4\pi D_{AB} R N_A + k}$$

$D_{AB}$  is the sum of the diffusion constants for species A and B,  $R$  is the reaction radius and  $k$  is the (second order) rate constant for complex formation when the molecules touch. When  $k \gg 4\pi D R N_A$ , the reaction is strictly diffusion controlled. The parameter  $k$  was fixed at  $k=1.2 \cdot 10^8 \text{M}^{-1} \text{s}^{-1}$  and the reaction radius at  $R=5 \text{nm}$ . The disassociation constant  $K_d = k_d/k_a$  was fixed at  $K_d=8.3 \cdot 10^{-8} \text{M}$ , which specifies how the dissociation rate constant,  $k_d$ , varies with  $k_a$ :

$$k_d = K_d k_a$$

The resulting rate constants are given in Table N1.  $k_1=150 \text{s}^{-1}$  and  $k_4=6 \text{s}^{-1}$  independent of diffusion constant.

D [ $\text{cm}^2 \text{s}^{-1}$ ]	$k_a$ [ $(\mu\text{M})^{-1} \text{s}^{-1}$ ]	$k_d$ [ $\text{s}^{-1}$ ]
<b><math>0.2 \cdot 10^{-8}</math></b>	<b>13.3</b>	<b>1.107</b>
<b><math>0.5 \cdot 10^{-8}</math></b>	<b>28.6</b>	<b>2.37</b>
<b><math>1.0 \cdot 10^{-8}</math></b>	<b>46.2</b>	<b>3.82</b>
<b><math>2.0 \cdot 10^{-8}</math></b>	<b>66.7</b>	<b>5.53</b>
<b><math>3.0 \cdot 10^{-8}</math></b>	<b>78.3</b>	<b>6.50</b>

Table N1.

### C. The rule for domain separation in 3D

To test the rule for domain separation and to determine the proportionality constant for the mixing time, we have varied the system parameters so that  $\tau_c$  is changing while the diffusion constant  $D$  and  $\tau_D$  is fixed (Fig. N3). Systems, for which  $\tau_c$  intersects  $\tau_D$  (colored curves), display domain separation, while systems without intersections (gray curves) do not.

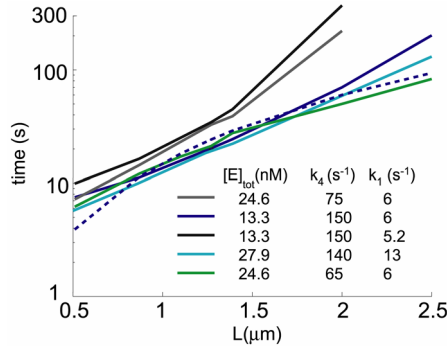


**Fig. N3. Parameter variations.** Solid lines are the correlation times for homogeneous systems of volume  $L^3$  with different parameters (see *insert*). The systems for which the dashed mixing time curve ( $3L^2/D$ ) intersects with the correlation time curve for some size of the systems ( $L^3$ ) display domain separation in a  $6 \times 6 \times 6 \mu\text{m}^3$  volume with periodic boundaries.

It can be noted that both  $\tau_c$  and  $\tau_D$  depend on diffusion, so that emergence of domain separation as a result of decreasing diffusion constants will take place in some, but not in other, types of systems. We have, for instance, been unable to identify a parameter set that allows for domain separation of the MAPK system in cubic volumes, although domain separation readily occurs when this system is extended in flat or linear geometries (see Text D).

## D. The MAPK system

We have simulated a dual MAPK phosphorylation-dephosphorylation cycle (Fig. N4). This simple system can display bi-stability without additional feed-back loops when the MAPKK and MKP operate distributive rather than processive [4]. The dephosphorylated MAPK (M) is phosphorylated in two steps by MAPKK; first to Mp and then to Mpp as follows [4]

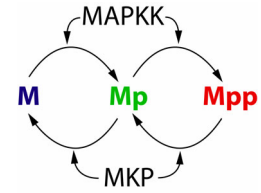
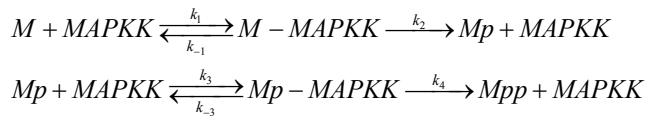
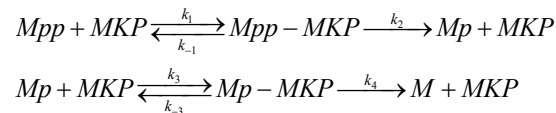


Fig. N4. MAPK phosphorylation-dephosphorylation cycle.

The rate constants were chosen as  $k_1=0.046 \text{ nM}^{-1}\text{s}^{-1}$ ,  $k_{-1}=1.8\text{s}^{-1}$ ,  $k_2=1.8\text{s}^{-1}$ ,  $k_3=0.046 \text{ nM}^{-1}\text{s}^{-1}$ ,  $k_{-3}=1.8\text{s}^{-1}$ ,  $k_4=50\text{s}^{-1}$  and the diffusion rate constant as  $D= 2 \cdot 10^{-8} \text{ cm}^2\text{s}^{-1}$ . The reaction rate constants are similar to those used in [4], where  $k_1=0.02 \text{ nM}^{-1}\text{s}^{-1}$ ,  $k_{-1}=1\text{s}^{-1}$ ,  $k_2=0.01\text{s}^{-1}$ ,  $k_3=0.032 \text{ nM}^{-1}\text{s}^{-1}$ ,  $k_{-3}=1\text{s}^{-1}$  and  $k_4=15\text{s}^{-1}$ . The main difference is that we have increased  $k_2$  towards the value of  $k_4$  in order to make the kinetics faster and  $\tau_1$  smaller. The dephosphorylation reactions are



In reference [4] an ordered dephosphorylation reaction was modeled, where the phosphotyrosine residue is dephosphorylated before the phosphothreonine residue. We have neglected the order of the reactions in order to keep the spatial model simple. To make the bi-stable system symmetrical, the same kinetic parameters were used in the dephosphorylation and phosphorylation schemes.

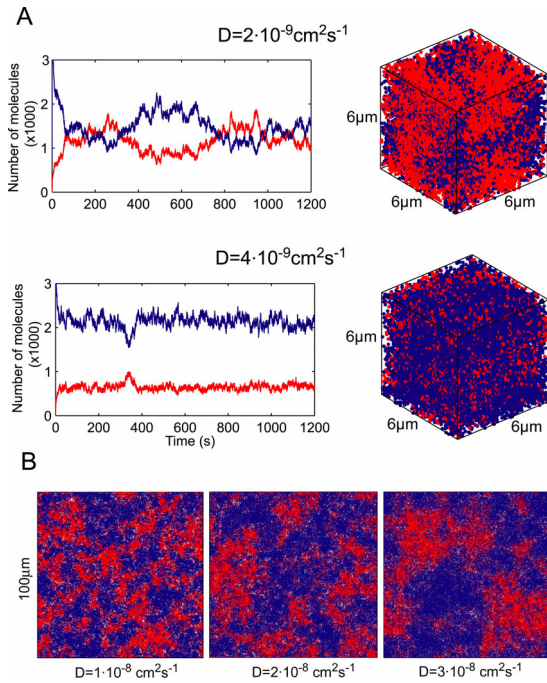
The total concentration of MAPK in all forms is 308nM. The total concentration of MAPKK and MKP is 50nM each. The simulations (Fig. 3, main text) were all done with  $10^6$  sub-volumes with  $\ell=0.1\mu\text{m}$ . Initially, all MAPKK and MKP are free, all MAPK is in the Mpp form (red) and all molecules are randomly distributed. No domain separation was seen for cube shaped volumes, but could be observed after about 100s when the system was contained in 1D or 2D like geometries.

## Supplementary References

1. Berg, O.G.: On diffusion-controlled dissociation, *Chemical Physics*, 1978, **31**:47-57.
2. Keizer, J.: *Statistical Thermodynamics of Nonequilibrium Processes*.(Springer-Verlag. Berlin, 1987).
3. Keizer, J.: Nonequilibrium Statistical Thermodynamics and the Effect of Diffusion on Chemical Reaction Rates, *J Phys Chem*, 1982, **86**:5052-5067.
4. Markevich, N.I., Hoek, J.B., and Kholodenko, B.N.: Signaling switches and bistability arising from multisite phosphorylation in protein kinase cascades, *J Cell Biol*, 2004, **164**:353-9.

# Supplementary Figure 1

## Domain separation in 3D with periodic boundaries



**A.** The figure illustrates the same system ( $6 \times 6 \times 6 \mu\text{m}$ ) as in Fig 1 in the main text, but with periodic boundaries. When  $D$  is  $2 \cdot 10^{-9} \text{ cm}^2 \text{ s}^{-1}$  (upper panels) the system displays domain separation (right) and the time evolution of the total number of molecules (left) does not show bistability. When  $D$  is  $4 \cdot 10^{-9} \text{ cm}^2 \text{ s}^{-1}$  (lower panels) there is no domain separation (right) and the system remains in one attractor for long times (left). Since boundaries are absent, patches with the system in opposite phase in the corners are also absent in contrast to the corresponding case with reflecting boundaries (Fig. 1B in main text).

**B.** Snap-shots of the distribution of molecules in a flat system ( $100 \times 100 \times 0.3 \mu\text{m}$ ) after fully developed domain separation. The system has periodic (toroidal) boundary conditions. The different diffusion constants are given in the figure.